Tribol Lett (2009) 36:277–284
DOI 10.1007/s11249-009-9512-9

ORIGINAL PAPER

# A Comparative Study of Residual Stress Distribution Induced by Hard Machining Versus Grinding

**Youngsik Choi**

Received: 31 May 2009 / Accepted: 24 August 2009 / Published online: 3 September 2009


**Abstract** This study investigates the residual stress distribution induced by hard machining and grinding and compares its impact on fatigue parameters. The residual stress distribution below hard turned and ground surfaces is investigated after a thermally damaged layer is removed. Fatigue parameters are computed based on the residual stress distribution to compare the impact of the residual stress distribution on the fatigue performance. Rolling contact fatigue tests are then performed to substantiate the computations. The effect of residual stresses on crack initiation depth is shown to be significant for the ground specimen. The maximum shear stress at crack initiation depth of the hard turned specimen is smaller than that of the ground specimen. Due to a significant increase in crack initiation life, the predicted rolling contact fatigue life of the hard turned specimen is longer than that of the ground specimen. The overall average in the ratios of predicted life to experimental life for the hard turned specimen is closer to 1 than that for the ground specimen. The results demonstrate that the hard turned specimen shows better rolling contact fatigue performance and better accuracy in the fatigue life prediction.

**Keywords** Turning · Grinding · Stress analysis · Rolling contact fatigue · Fatigue analysis

Y. Choi (✉)
Department of Mechanical and Aerospace Engineering, Florida Institute of Technology, Melbourne, FL 32901, USA
e-mail: choi@fit.edu

## 1 Introduction

Hard machining and grinding are competitive process for making precision components. Typically, hard machining and grinding produce different surface integrity due to the process features. Hard machining has advantages over grinding in terms of setup time, processing time, number of processes, material handling time, equipment cost, and system flexibility.

Since surface integrity usually determines the service life of structural components, an extensive understanding of surface integrity aspects is demanded to implement hard machining as a finishing process. Surface integrity, which involves the inherited or altered properties of a surface produced by manufacturing processes, includes residual stress, micro hardness, surface finish, and microstructure.

Abrão and Aspinwall [1] investigated the surface integrity of hard turned and ground bearing steel. The study revealed that hard turning induces more compressive residual stresses than grinding. Matsumoto et al. [2] compared residual stress profiles produced by hard turning and grinding. They indicated that hard turning induces maximum compressive residual stress at the subsurface, while grinding induces maximum compressive residual stress at the surface.

König et al. [3] investigated the surface integrity of hard turned bearing steel. They found that a more aggressive infeed increases the depth of the affected zone and the level of compressive residual stresses. Hua et al. [4] investigated the effect of cutting conditions and cutting edge preparations on subsurface residual stresses of hard turned bearing steel. They noted that an optimal tool edge geometry and aggressive feedrate increase compressive residual stresses.

Since residual stresses produced by hard machining are more deterministic than those by grinding, there have been

attempts to model residual stresses of hard turned surfaces. Mittal and Liu [5] put forward a residual stress model, reporting that the use of the model to refine manufacturing processes can enhance the rolling contact fatigue performance of hard turned components.

Liu and Guo [6] carried out a finite element simulation of residual stresses produced by hard turning and demonstrated that residual stresses of a hard turned surface can be changed to a better state by optimizing the second cut. A residual stress model based on back-propagation neural network was developed by Zhang et al. [7], and the model could predict residual stress profiles of hard turned surfaces more accurately than conventional linear regression method.

Nakayama et al. [8] investigated surface finish of hard turned and ground surfaces. The study revealed that surface finish of hard turned surfaces is at least as good as that of ground surfaces as a result of minimal plastic flow and the absence of a built-up edge due to the high hardness of material. Davies et al. [9] further investigated this finding in hard turning of AISI 52100 steel and surface finish was found to deteriorate with the increase of tool flank wear.

Hard turning and grinding can produce a rehardening burn layer at the machined surface that is resistant to etching in contrast to the bulk material; hence, commonly called a "White Layer." A white layer produced by hard turning is typically less than 12 μm [10], while one produced by grinding can reach 100 μm [11].

Matsumoto et al. [12] investigated the microstructure of hard turned steel and noted that a white layer is observed in the case of machining with a ceramic chamfered tool, while this layer is not visible in the case of machining with a sharp tool. Tonshoff et al. [10] investigated the chemical composition of ASTM 5115 steel when white layers were produced by hard machining. They reported that no element concentration transition from the over-tempered layer to white layers was found.

Guo and Janowski [13] compared the microstructure of white layers produced by hard turning and grinding. They reported that a mechanical deformation is dominant in white layer formation by hard turning, while a thermal process is dominant in white layer formation by grinding.

Liu and Mittal [14] studied the feasibility of replacing abrasion-based superfinishing with hard turning and demonstrated that hard turning can produce even better surface integrity than abrasion-based superfinishing. Agha and Liu [15] did an experimental study on the rolling contact fatigue performance of hard turned and ground surfaces. They found that the deterministic nature of hard turning results in more consistent repeatability of the rolling contact fatigue life. Liu and Mittal [16] presented a method to maximize the rolling contact fatigue life of hard turned surfaces. They indicated that the selection of machining parameters can greatly affect the rolling contact fatigue life.

Although general surface integrity factors of hard machined or ground surfaces have been investigated, the specific difference in fatigue parameters solely due to the residual stress distribution induced by hard machining and grinding has not yet been explored. Since machining-induced residual stresses are of great importance in fatigue performance, this study investigates the residual stress distribution induced by hard machining and grinding and compares its impact on fatigue parameters.

After a thermally damaged layer is removed, the residual stress distribution below hard turned and ground surfaces is investigated. Fatigue parameters are computed based on the residual stress distribution to compare the impact of the residual stress distribution on the fatigue performance. Then, rolling contact fatigue tests are performed to substantiate the computations.

## 2 Experimental

Specimens of through hardened AISI 1053 steel were prepared for the experiment, since this steel is used for bearing applications. The composition of AISI 1053 steel is given in Table 1. Figure 1 shows the dimensions of the specimen, which were selected to minimize deflection by the chucking forces of a standard jaw and to be uniformly through hardened [17].

### 2.1 Machining Conditions

For a pair of specimens, the flat surfaces were turned by using a cubic boron nitride (CBN) tool at the machining conditions shown in Table 2. A layer of 100 μm thickness was then removed by an etching to remove a thermally damaged layer. The thickness of removed layer by an etching was determined based on previous research [18].

For another pair of specimens, the flat surfaces were ground in a sequence of three cuts of 51 μm, followed by two cuts of 25 μm, two cuts of 13 μm, and one cut of 5 μm. Table 3 lists the grinding conditions, which were selected to induce less thermal damage and less residual stress below the ground surface [19]. A layer of 50 μm thickness was then removed by an etching to remove a thermally damaged layer. The thickness of removed layer

**Table 1** Composition (%) of specimens

| Material | C | Mn | P | S |
|---|---|---|---|---|
| AISI 1053 | 0.48–0.55 | 0.70–1.00 | 0.04 | 0.05 |

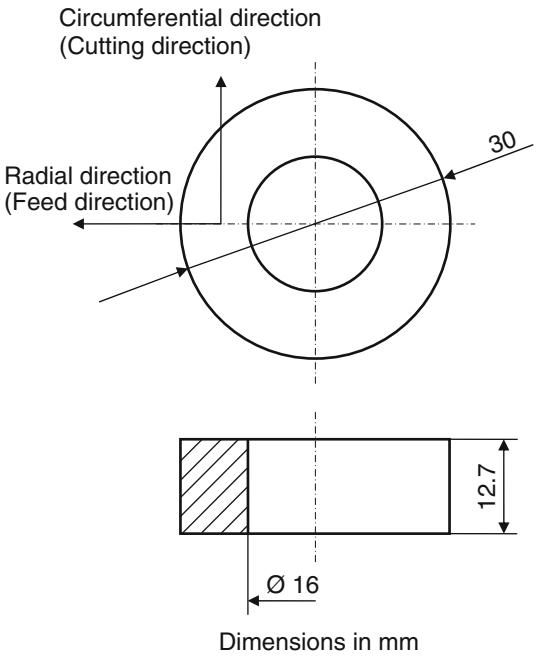


**Fig. 1** Dimensions of specimen

**Table 2** Hard turning conditions

| Parameter | Description |
|---|---|
| Cutting speed | 2.11 m/s |
| Feedrate | 0.08 mm/rev |
| Depth of cut | 0.127 mm |
| Coolant | Dry |
| Rake angle | −5° |

**Table 3** Grinding conditions

| Parameter | Description |
|---|---|
| Wheel speed | 1800 rpm |
| Table speed | 18.3 m/min |
| Cross feed | 1.27 mm |
| Lubricant | Sulfo-chlorinated oil |
| Wheel specification | 82A34L8VBE |
| Depth of cut | 51, 25, 13, and 5 μm |

by an etching was 10 times the depth of cut of the last pass in grinding.

## 2.2 Residual Stress Measurement

X-ray diffraction was used to measure the residual stress distribution in the subsurface of specimens. A GE XRD-5 diffractometer was used with a CrKα radiation tube. The $\sin^2\psi$ technique was applied to compute the residual stress value [20].

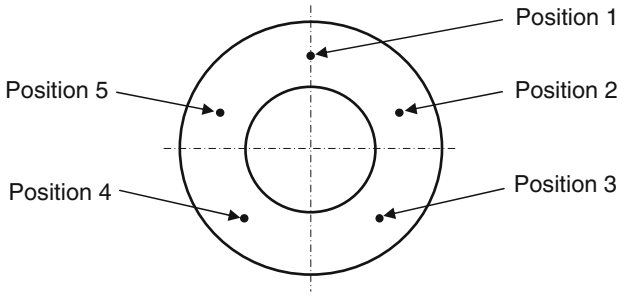


**Fig. 2** Positions of residual stress measurement

**Table 4** Repeatability of residual stress measurement

| Reading | Residual stress (MPa) |
|---|---|
| 1 | −403.64 |
| 2 | −410.00 |
| 3 | −410.00 |
| 4 | −402.05 |
| 5 | −406.82 |
| 6 | −405.23 |
| 7 | −400.47 |
| 8 | −394.11 |
| Average | −404.04 |
| SD | 5.3 |

The measurements were made at the exposed surface and six different depths below the surface: 2.54, 5.08, 7.62, 10.16, 12.7, and 25.4 μm. To investigate the residual stress scatter, the measurements were made at five different positions at each depth (Fig. 2). To measure residual stresses at different depths, a layer was removed with the help of an electrolytic etcher, saturated NaCl solution. The thickness of the specimen was measured to check the removed depth of a layer after each etching.

The same point on the same specimen was measured eight times by loading and unloading the specimen in the X-ray diffractometer to evaluate the repeatability of residual stress measurements. Table 4 demonstrates that the measurement readings show good consistency [21].

## 2.3 Rolling Contact Fatigue Test

The rolling contact fatigue test was performed by using a special test rig in a temperature-controlled room set to 25 °C. The thrust ball bearing, which has Grade 25 balls of 3.69 mm diameter, was inserted between two specimens. The upper specimen was rotated at 1840 rpm, and the lower specimen was fixed in the test rig. An axial load that produces a maximum Hertzian stress of 2720 MPa was imposed on the upper specimen.

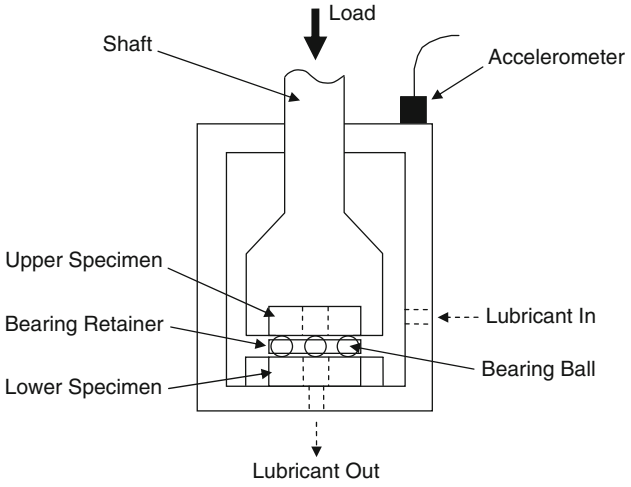


**Fig. 3** Schematic diagram of a rolling contact fatigue test rig

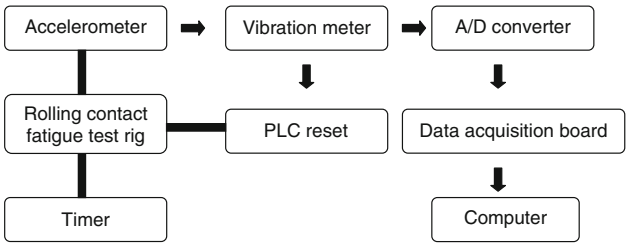


**Fig. 4** Data acquisition system setup

The bearing and the rolling contact specimens were immersed in SAE-30 lubrication oil, which was circulated through a 0.25 μm filtered-pump feed system at a rate of 56.8 $cm^3$/min, while a test was run. Figure 3 shows a schematic diagram of the rolling contact fatigue test rig. It was reported that the experimental lives by this test rig show less than 10–17% differences with those by the Falex multi-specimen rolling fatigue tester [15].

The rolling contact fatigue test was monitored by an accelerometer connected to a vibration meter. The vibration signal, which is influenced by both the upper and the lower specimens, was acquired by the data acquisition system (Fig. 4). When the vibration level reached a threshold level, the test rig and the timer were stopped by a PLC reset. To detect the initiation of a fatigue spall, the vibration threshold level was set to 0.2 g. For each specimen, the fatigue test was performed thrice, and the average of those was taken as measurement data.

## 3 Prediction of Rolling Contact Fatigue Life

Rolling contact fatigue for properly lubricated conditions normally begins with crack initiation in the subsurface. The cracks then propagate by a continued rolling, eventually reaching the exposed surface. Afterward, surface fragments are dislodged, which results in the initiation of a fatigue spall.

Choi and Liu [22] proposed a crack initiation life model and a crack propagation life model to predict the initiation of a fatigue spall. Liu and Choi [23] later developed a crack initiation life model based on a dislocation model, and this model showed better accuracy than their previous model. To predict the fatigue life, the crack initiation life model based on a dislocation model [23] and the crack propagation life model [22] are combined in this article.

### 3.1 Crack Initiation Life Model

The crack initiation life model was developed by using a dislocation model [23]. Based on previous finding [24], the maximum shear stress replaces the local shear stress in the dislocation model, and the crack initiation point is assumed to be where the ratio of the maximum shear stress to hardness is highest.

Accordingly, the crack initiation life model can be written as:

$$N_i = \frac{I}{(\Delta\tau_{\max} - 2\tau_k)^2} \tag{1}$$

where $N_i$ is the number of loading cycles to crack initiation, $I$ the initiation constant, $\Delta\tau_{\max}$ the range of maximum shear stress incorporating residual stresses during a cycle at the initiation point, and $\tau_k$ is the frictional stress at the initiation point.

### 3.2 Crack Propagation Life Model

The crack propagation life model was developed by using the modified Paris' formula [22]. Paris and Erdogan [25] proposed a formula for the correlation between the crack propagation rate and the stress intensity factor range. Chen et al. [26] measured crack propagation rates during the rolling contact fatigue test and noted that the crack propagates relatively faster as the local hardness is lower if the stress field is identical. Paris' formula is modified accordingly.

By integrating the crack propagation rate from the initial crack size to the final crack size, the crack propagation life model can be written as

$$N_p = \int_{a_1}^{a_2} \frac{1}{C\frac{H_b}{H_l}(\Delta K)^n} \mathrm{d}a \tag{2}$$

where $N_p$ is the crack propagation life in loading cycles, $a_1$ the half length of the initial crack size, $a_2$ the half length of the final crack size, $C$ the material constant, $H_b$ the Knoop Hardness number at the bulk material, $H_l$ the local Knoop

Hardness number, $\Delta K$ the stress intensity factor range at the leading tip, $n$ the slope index, and $a$ is the half length of the crack.

### 3.3 Rolling Contact Fatigue Life Model

The crack initiation life model is combined with the crack propagation life model to predict the fatigue life as follows:

$$N = \frac{I}{(\Delta\tau_{\max} - 2\tau_k)^2} + \int_{a_1}^{a_2} \frac{1}{C\frac{H_b}{H_l}(\Delta K)^n}\,\mathrm{d}a \qquad (3)$$

where $N$ is the fatigue life in loading cycles.

## 4 Results and Discussion

The residual stress distribution of the hard turned specimen is shown in Fig. 5. Residual stresses vary depending on the depth for the same position and show some variation at the same depth depending on the position. The peak compressive residual stress is typically located at the depth of 10.16 μm and ranges between 820 and 880 MPa.

The residual stress distribution of the ground specimen is shown in Fig. 6 [27]. Residual stresses vary significantly depending on the depth for the same position and show a wide variation even at the same depth depending on the position. It is noted that the variation is more significant than the hard turned specimen. The peak compressive residual stress is typically located at the depth of 25.4 μm and ranges between 460 and 750 MPa.

Since residual stresses vary depending on the position, the residual stress measurements at all the positions are considered for the prediction of fatigue life. Since the residual stress of the specimen before machining was found to be a constant compressive stress of 800 MPa [28], it is conceivable that the residual stress scatter stems from machining processes.

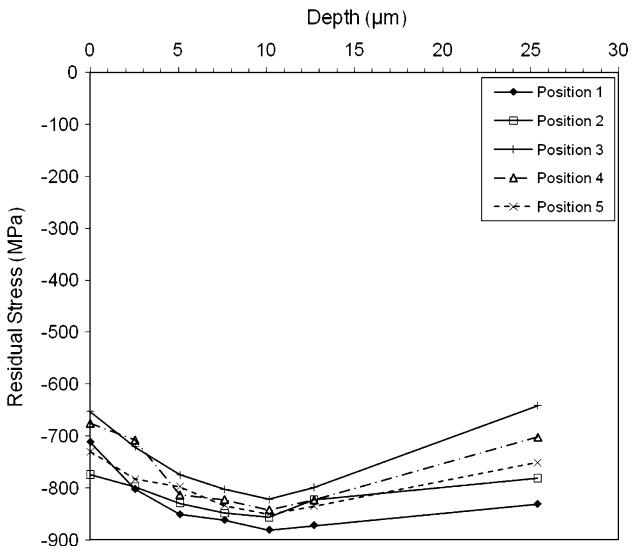


**Fig. 5** Residual stress distribution of hard turned specimen

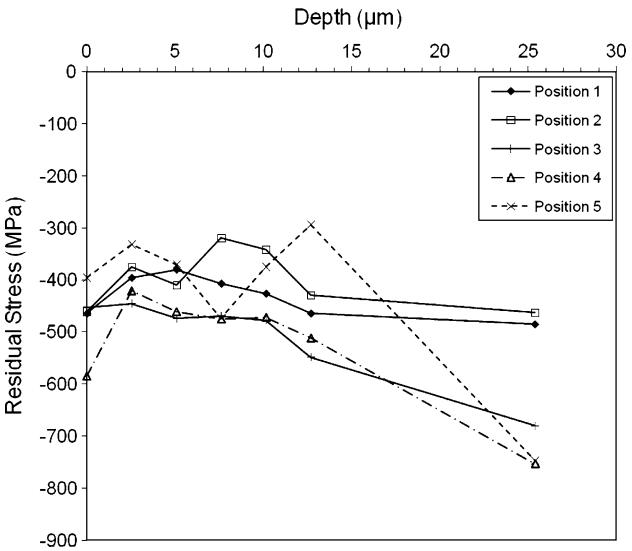


**Fig. 6** Residual stress distribution of ground specimen

### 4.1 Computed Crack Initiation Depth

The crack initiation depth was computed based on subsurface stress distribution. The crack initiation depths are shown in Fig. 7. Depending on the position, the crack initiation depth of the hard turned specimen is nearly constant, while that of the ground specimen varies appreciably. Generally, the crack initiation depth of the hard turned specimen is deeper than that of the ground specimen.

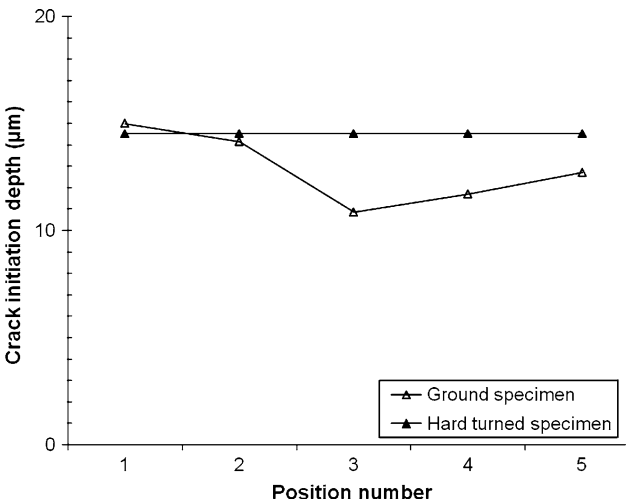


**Fig. 7** Crack initiation depth comparison

Before residual stresses were taken into account, the crack initiation depth was found to be 14.5 μm by locating where the maximum shear stress is highest. For the ground specimen, the effect of residual stresses on crack initiation depth is shown to be significant considering that the crack initiation depth is 14.5 μm before residual stresses are taken into account. However, the effect of residual stresses on crack initiation depth is shown to be negligible for the hard turned specimen.

The crack initiation depth affects the fatigue performance considerably as the initial spall size and the crack propagation length required to reach the exposed surface are dependent on the crack initiation depth. The initial spall size determines a number of continued loading cycles required to increase the spall size for the final failure. The crack propagation length required to reach the exposed surface determines the crack propagation life as long as the stress field is identical.

### 4.2 Computed Maximum Shear Stress at Crack Initiation Depth

The maximum shear stress at crack initiation depth was computed and shown in Fig. 8. The maximum shear stress of both the hard turned specimens and the ground specimens varies appreciably depending on the position.

Typically, the maximum shear stress of the hard turned specimen is smaller than that of the ground specimen. It is noted that both hard turning and grinding reduce the maximum shear stress at crack initiation depth, considering that the maximum shear stress is 678.6 MPa before residual stresses are taken into account.

For the hard turned specimen, the maximum shear stress is reduced to as low as 294.8 MPa, which demonstrates that about 57% of maximum shear stress can be reduced by hard turning. For the ground specimen, the maximum shear stress is reduced to as low as 413.2 MPa, which demonstrates that about 39% of maximum shear stress can be reduced by grinding. The effect of hard turning or grinding on crack initiation life is expected to be significant considering that the maximum shear stress is a key value for crack initiation life.

### 4.3 Prediction of Rolling Contact Fatigue Life

The rolling contact fatigue life was predicted by using the rolling contact fatigue life model (Eq. 3). The predicted lives are shown in Fig. 9. Choi and Liu [29] developed a spall progression life model and verified it experimentally. They revealed that the spall progression life covers a significant portion in the rolling contact fatigue life. Since the fatigue life predicted by Eq. 3 is the summation of crack initiation life and crack propagation life, it is lower than a general fatigue life which includes crack initiation life, crack propagation life, and spall progression life.

Typically, the fatigue life of the hard turned specimen is longer than that of the ground specimen. The longest fatigue life of the hard turned specimen is around 14 times that of the ground specimen. The fatigue life of the hard turned specimen varies significantly depending on the position, while that of the ground specimen is nearly constant. This is due to a significant variation in crack initiation life for the hard turned specimen. The crack initiation life is more sensitive to the maximum shear stress as the maximum shear stress decreases. Furthermore, the crack initiation life covered more than 90% of the fatigue life for the hard turned specimen, while it covered about 70% of the fatigue life for the ground specimen.

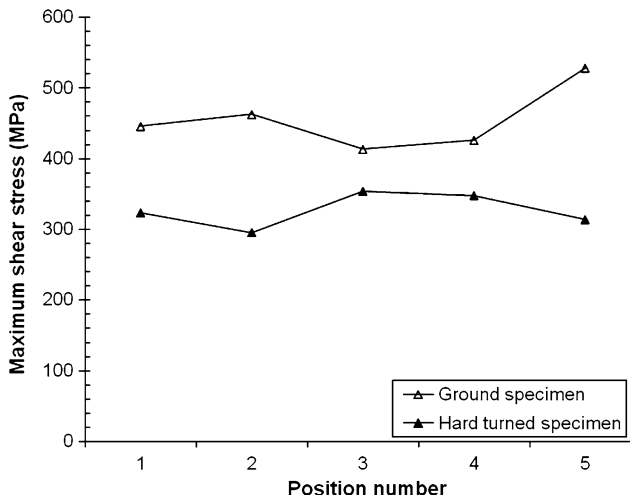


**Fig. 8** Maximum shear stress comparison

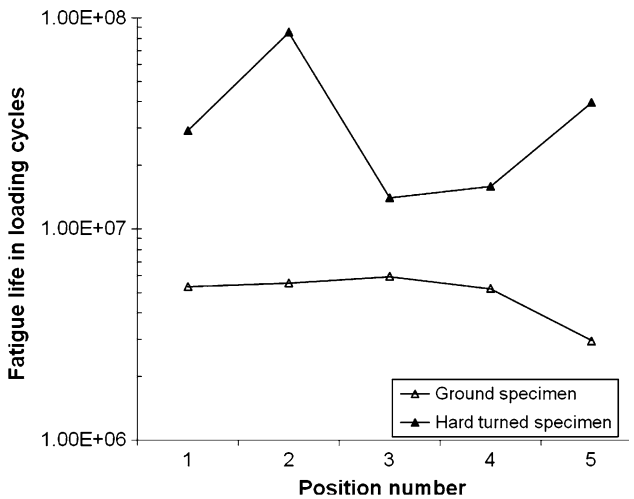


**Fig. 9** Predicted fatigue life comparison

**Table 5** Ratio of predicted life to experimental life

| Position | Ratio of predicted life to experimental life | |
|---|---|---|
| | Ground specimen | Hard turned specimen |
| 1 | 2.39 | 1.35 |
| 2 | 2.49 | 3.94 |
| 3 | 2.68 | 0.65 |
| 4 | 2.35 | 0.73 |
| 5 | 1.33 | 1.83 |
| Average | 2.25 | 1.70 |
| SD | 0.53 | 1.34 |

### 4.4 Rolling Contact Fatigue Test

The ratio of predicted life to experimental life was calculated for the ground and the hard turned specimens (Table 5). The overall average in the ratios for the hard turned specimen is closer to 1 than that for the ground specimen, while the standard deviation for the hard turned specimen is larger than that for the ground specimen as all the predicted lives for the ground specimen are over-predictions.

The results demonstrate that the hard turned specimen shows better rolling contact fatigue performance than the ground specimen due to a significant increase in crack initiation life, and that the hard turned specimen shows better accuracy in the fatigue life prediction than the ground specimen in terms of the overall average in the ratios.

## 5 Conclusions

The residual stress distribution below hard turned and ground surfaces was investigated after a thermally damaged layer was removed. Based on the residual stress distribution, fatigue parameters were computed to compare the impact of the residual stress distribution on the fatigue performance.

Residual stresses of the ground specimen varied significantly depending on the depth for the same position and showed a wide variation even at the same depth depending on the position, while the residual stress variation of the hard turned specimen was relatively insignificant.

Typically, the peak compressive residual stress of the hard turned specimen was located at the depth of 10.16 μm, while that of the ground specimen was located at the depth of 25.4 μm. The peak compressive residual stress of the hard turned specimen ranged between 820 and 880 MPa, while that of the ground specimen ranged between 460 and 750 MPa.

The crack initiation depth of the hard turned specimen was generally deeper than that of the ground specimen. Depending on the position, the crack initiation depth of the hard turned specimen was nearly constant, while that of the ground specimen varied appreciably. The effect of residual stresses on crack initiation depth was significant for the ground specimen, while negligible for the hard turned specimen.

The maximum shear stress at crack initiation depth for both the hard turned and the ground specimens varied appreciably depending on the position. Both the hard turning and the grinding reduced the maximum shear stress at crack initiation depth, while the maximum shear stress at crack initiation depth of the hard turned specimen was smaller than that of the ground specimen.

The predicted rolling contact fatigue life of the hard turned specimen was longer than that of the ground specimen. The longest predicted life of the hard turned specimen was around 14 times that of the ground specimen. The predicted life of the hard turned specimen varied significantly, while that of the ground specimen was nearly constant depending on the position.

The overall average in the ratios of predicted life to experimental life for the hard turned specimen was closer to 1 than that for the ground specimen, while the standard deviation for the hard turned specimen was larger than that for the ground specimen as all the predicted lives for the ground specimen were over-predictions.

The results demonstrate that the hard turned specimen shows better rolling contact fatigue performance and better accuracy in the fatigue life prediction than the ground specimen.

## References

1. Abrão, A.M., Aspinwall, D.K.: The surface integrity of turned and ground hardened bearing steel. Wear **196**, 279–284 (1996)
2. Matsumoto, Y., Hashimoto, F., Lahoti, G.: Surface integrity generated by precision hard turning. CIRP Ann. **48**, 59–62 (1999)
3. König, W., Klinger, M., Link, R.: Machining hard materials with geometrically defined cutting edges-Field of applications and limitations. CIRP Ann. **39**, 61–64 (1990)
4. Hua, J., Umbrello, D., Shivpuri, R.: Investigation of cutting conditions and cutting edge preparations for enhanced compressive subsurface residual stress in the hard turning of bearing steel. J. Mater. Process. Technol. **171**, 180–187 (2006)
5. Mittal, S., Liu, C.R.: A method of modeling residual stress in superfinish hard turning. Wear **218**, 21–33 (1998)
6. Liu, C.R., Guo, Y.B.: Finite element analysis of the effect of sequential cuts and tool-chip friction on residual stresses in a machined layer. Int. J. Mech. Sci. **42**, 1069–1089 (2000)
7. Zhang, J.Y., Liang, S.Y., Zhang, G., Yen, D.: Modeling of residual stress profile in finish hard turning. Mater. Manuf. Process. **21**, 39–45 (2006)

8. Nakayama, K., Aria, M., Kanda, T.: Machining characteristics of hard materials. CIRP Ann. **37**, 89–92 (1988)
9. Davies, M.A., Chou, Y., Evans, C.J.: On chip morphology, tool wear, and cutting mechanics in finish hard turning. CIRP Ann. **45**, 77–82 (1996)
10. Tonshoff, H.K., Wobker, H.G., Brandt, D.: Hard turning-Influences on the workpiece properties. Trans. NAMRI/SME **23**, 215–220 (1995)
11. Eda, H., Kishi, K., Hashimoto, S.: The formation mechanism of ground white layers. JSME Bull. **24**, 743–747 (1981)
12. Matsumoto, Y., Barash, M.M., Liu, C.R.: Cutting mechanism during machining of hardened steel. Mater. Sci. Technol. **3**, 299–305 (1987)
13. Guo, Y.B., Janowski, G.M.: Microstructural characterization of white layers by hard turning and grinding. Trans. NAMRI/SME **32**, 367–374 (2004)
14. Liu, C.R., Mittal, S.: Single-step superfinish hard machining-Feasibility and feasible cutting conditions. Robot. Comp. Integr. Manuf. **12**, 15–27 (1996)
15. Agha, S.R., Liu, C.R.: Experimental study on the performance of superfinish hard turned surfaces in rolling contact. Wear **244**, 52–59 (2000)
16. Liu, C.R., Mittal, S.: Optimal pre-stressing the surface of a component by superfinish hard turning for maximum fatigue life in rolling contact. Wear **219**, 128–140 (1998)
17. Agha, S.R.: Fatigue performance of superfinish hard turned surfaces in rolling contact. Ph.D. Thesis, Purdue University (2000)
18. Choi, Y., Liu, C.R.: Rolling contact fatigue life of finish hard machined surfaces—part 2. Experimental verification. Wear **261**, 492–499 (2006)
19. Bellows, G.: Low Stress Grinding for Quality Production. Machinability Data Center, Cincinnati (1978)
20. Noyan, I.C., Cohen, J.B.: Residual Stress-Measurement by Diffraction and Interpretation. Springer, New York (1987)
21. Martell, J.J.: Surface integrity variation in machined surfaces. MS Thesis, Purdue University (2007)
22. Choi, Y., Liu, C.R.: Rolling contact fatigue life of finish hard machined surfaces—part 1. Model development. Wear **261**, 485–491 (2006)
23. Liu, C.R., Choi, Y.: A new methodology for predicting crack initiation life for rolling contact fatigue based on dislocation and crack propagation. Int. J. Mech. Sci. **50**, 117–123 (2008)
24. Leng, X., Chen, Q., Shao, E.: Initiation and propagation of case crushing cracks in rolling contact fatigue. Wear **122**, 33–43 (1988)
25. Paris, P., Erdogan, F.: A critical analysis of crack propagation laws. Trans. ASME J. Basic Eng. **85**, 528–534 (1963)
26. Chen, Q., Leng, X., Shao, E.: Influence of microstructure and residual stress on the stages of case crushing. Wear **122**, 45–55 (1988)
27. Liu, C.R., Choi, Y.: Rolling contact fatigue life model incorporating residual stress scatter. Int. J. Mech. Sci. **50**, 1572–1577 (2008)
28. Shunmugam, R.: Application of Taguchi methods for cutting parameters selection in hard turning. MS Thesis, Purdue University (2004)
29. Choi, Y., Liu, C.R.: Spall progression life model for rolling contact verified by finish hard machined surfaces. Wear **262**, 24–'35 (2007)